University of New Hampshire
University of New Hampshire Scholars' Repository

Physics Scholarship | Physics

6-5-2009

A novel metric for coronal MHD models

D. J. Schmit

S. Gibson

G. De Toma

M. Wiltberger

W. J. Hughes

See next page for additional authors

Follow this and additional works at: http://scholars.unh.edu/physics_facpub

 Part of the Physics Commons

Recommended Citation

Schmit, D. J., S. Gibson, G. de Toma, M. Wiltberger, W. J. Hughes, H. Spence, P. Riley, J. A. Linker, and Z. Mikic (2009), A novel metric for coronal MHD models, J. Geophys. Res., 114, A06101, doi:10.1029/2008JA013732.

This Article is brought to you for free and open access by the Physics at University of New Hampshire Scholars' Repository. It has been accepted for inclusion in Physics Scholarship by an authorized administrator of University of New Hampshire Scholars' Repository. For more information, please contact nicole.hentz@unh.edu.

A novel metric for coronal MHD models

Rights
Copyright 2009 by the American Geophysical Union.

Authors
D. J. Schmit, S. Gibson, G. De Toma, M. Wiltberger, W. J. Hughes, Harlan E. Spence, P. Riley, J. A. Linker, and Z. Mikic

This article is available at University of New Hampshire Scholars' Repository: http://scholars.unh.edu/physics_facpub/203

A novel metric for coronal MHD models

D. J. Schmit,[1] S. Gibson,[2] G. de Toma,[2] M. Wiltberger,[2] W. J. Hughes,[3] H. Spence,[3] P. Riley,[4,5] J. A. Linker,[4,5] and Z. Mikic[4,5]

Received 5 September 2008; revised 4 February 2009; accepted 3 April 2009; published 5 June 2009.

[1] In the interest of quantitatively assessing the capabilities of coronal MHD models, we have developed a metric that compares the structures of the white light corona observed with SOHO LASCO C2 to model predictions. The MAS model is compared to C2 observations from two Carrington rotations during solar cycle 23, CR1913 and CR1984, which were near the minimum and maximum of solar activity, respectively, for three radial heights, 2.5 $R_\odot$, 3.0 $R_\odot$, and 4.5 $R_\odot$. In addition to simulated polarization brightness images, we create a synthetic image based on the field topology along the line of sight in the model. This open-closed brightness is also compared to LASCO C2 after renormalization. In general, the model's magnetic structure is a closer match to observed coronal structures than the model's density structure. This is expected from the simplified energy equations used in current global corona MHD models.

Citation: Schmit, D. J., S. Gibson, G. de Toma, M. Wiltberger, W. J. Hughes, H. Spence, P. Riley, J. A. Linker, and Z. Mikic (2009), A novel metric for coronal MHD models, *J. Geophys. Res.*, *114*, A06101, doi:10.1029/2008JA013732.

1. Introduction

[2] The solar atmosphere plays a fundamental role in the Sun-Earth system. The corona is the source of the solar wind, and it is the variability of the solar wind that drives much of the phenomena that define the state of Earth's space environment. In recent years, the space physics community has invested effort into linking together many models which simulate distinct parts of the Sun-Earth system, in the interest of creating a comprehensive space weather model. The Center for Integrated Space weather Modeling (CISM) is a NSF Science and Technology Center devoted to this task. The driving inner boundary of these models lies in the solar corona. In order to obtain accurate solutions throughout the whole system, it is essential to be able to assess the capabilities of the coronal model through a metric. A metric is a quantitative method that accurately describes how well a model is able to reproduce physical observations. Metrics present the goodness of fit of a model. By defining an appropriate metric, an objective comparison of models can be made and individual model improvements can be can be tracked as their physics are augmented over time. A comprehensive discussion on metrics and their role in CISM can be found in the work of *Spence et al.* [2004].

[3] Coronal and heliospheric metrics are limited by data sources which can be compared with models. Past attempts have focused on solar wind in situ data [*Owens et al.*, 2005; *McGregor et al.*, 2008; *Lee et al.*, 2009]. We have defined a coronal metric based on polarized brightness (pB) white light coronagraph observations. The pB images yield information on both the electron density and magnetic structures of the corona, which can be used to constrain and test MHD models of the corona. In this paper, the metric is applied to the Magnetohydrodynamics Around a Sphere (MAS) model [*Linker et al.*, 1999], which outputs both the density and vector magnetic field for the global corona.

[4] In section 2, the MAS model is described along with the SOHO LASCO white light coronagraph data and our method of constructing a metric. In section 3, the results of applying this metric are presented for two time periods, one during solar minimum and the other at solar maximum. In section 4, the implications and significance of the metric results are discussed.

2. Methodology

2.1. MAS Model

[5] The Magnetohydrodynamics Around a Sphere model [*Linker et al.*, 1999; *Riley et al.*, 2006a, 2006b, 2002] solves the viscous, resistive MHD equations for a spherical grid. Detailed discussion of the equations and computational method is found in [*Linker et al.*, 1999]. The energy equation is simplified using a polytrope approximation which does not include energy sources. In this paper γ is set to 1.05, which is nearly isothermal and significantly smaller than the physical adiabatic value of 5/3. This simplification inherently limits the model's ability to quantify density structures in the corona.

[6] The particular version of MAS used in this study solves the MHD equations to steady state for the global

[1]Department of Astrophysical and Planetary Science, University of Colorado, Boulder, Colorado, USA.
[2]High Altitude Observatory, National Center for Atmospheric Research, Boulder, Colorado, USA.
[3]Center for Space Physics, Boston University, Boston, Massachusetts, USA.
[4]Scientific Corporation International Corporation, San Diego, California, USA.
[5]Now at Solar Physics Group, Predictive Science Incorporated, San Diego, California, USA.

Copyright 2009 by the American Geophysical Union.
0148-0227/09/2008JA013732

corona. Because of the large scale domain the model grid is defined so as to capture large scale structures. There are $64 \times 70 \times 70$ cells in the (r, θ, ϕ) directions. The radial domain is 1 $R_\odot$ to 30 $R_\odot$. The grid is finer near the equator and in the inner corona so as to capture more precisely these dynamical areas.

[7] The boundary conditions of the model specify a uniform density and temperature at the inner boundary. The magnetic field is initiated with a potential field extrapolation based on line-of-sight (LOS) photospheric synoptic magnetograms of a full solar rotation ($\sim$27 days) from the National Solar Observatory at Kitt Peak.

2.2. Polarization Brightness

[8] Observations of the outer corona are primarily obtained by white light coronagraphs. It is difficult to directly determine the density distribution in the corona since the signal obtained is a superposition of structures integrated along the LOS in the optically thin corona. Therefore to compare MHD simulations of the corona to observations the white light intensity is calculated by integrating the three-dimensional density model output along the LOS. The white light K-corona is produced by photospheric light Thomson scattered by coronal electrons. White light coronal brightness also contains contributions from zodiacal light, known as the F-corona. Because the F-corona is largely unpolarized below 5 solar radii [*Saito et al.*, 1977] and the K-corona is highly polarized, it is useful to use observations of polarization brightness (pB) to isolate the K-corona. The pB is the difference in intensity of radiation polarized tangential to the limb of the Sun and radiation polarized normal to the limb. In particular, polarization brightness can be calculated from the number density using,

$$pB = \frac{\pi \sigma r_\odot B_\odot}{2} \int_{-\pi/2}^{\pi/2} n[(1-u)A + uB] d\theta \qquad (1)$$

where $B_\odot$ is the mean photospheric brightness, u is the limb darkening constant, σ is the Thomson scattering cross section of an electron, n is the local electron density, and θ is the angle between Sun center and points along the LOS. A and B are functions of θ and are derived via the integration of photon source angle over a hemisphere of the Sun. *Billings* [1966] and *Hundhausen* [1993] derive this LOS scattering integral and provide analytic examples.

[9] The pB data used in this paper comes from the SOHO LASCO C2 coronagraph which observes the solar corona between 2 and 6 $R_\odot$. On average LASCO C2 makes one pB observation each day using a polarization filter. An example of C2 data is shown in Figures 1a and 1d, in the form of a Carrington map. Carrington maps are formed by synoptically piecing together several days worth of observations at a set radial height over one solar rotation, which is slightly over 27 days long. In this sense, the Carrington longitude of the limb is synonymous with the date of the observation. Carrington maps make it possible to examine the global structure of the corona by reducing the data from a full solar rotation to a single image. Observational and simulated Carrington maps present the data in a form convenient for quantitatively assessing the capabilities of the model at capturing coronal structures.

2.3. Designing a Metric

[10] The pB scattering LOS integral is applied to the steady state density solution from the MAS model and produces simulated pB (spB) images which are directly comparable to LASCO C2 coronagraph data. Images corresponding to particular dates are created by matching that day's meridional longitude and solar B angle. Examples are shown in Figures 1b and 1e. However, in light of the simplified energy equations used by contemporary MHD models we do not expect the density structures in the models to quantitatively match coronal observations. Consequentially, an alternative approach is chosen in addition where simulated LOS scattering images are created using the magnetic structures predicted by the model.

[11] Open-closed brightness (ocB) images are formed by categorizing the corona into open or closed regions based on their magnetic topology. The vector magnetic field output of the model is used to trace field lines for each point in the model grid. By examining the location of foot points of the field lines it is determined whether field lines are open or closed. To first order approximation, the corona can be divided into regions that are either magnetically open and in hydrodynamic Parker equilibrium or closed and in hydrostatic equilibrium. Because the magnetic field dictates the movement of the plasma, the open field regions are of much lower density than the closed regions where the plasma is confined within magnetic loops. Based on these principles, as field lines within the model grid are traced, a proxy density of binary value, 0 or 1, is assigned to points of open and closed magnetic configuration respectively. By applying the pB integration discussed above to this proxy density field, ocB images are constructed. Examples of these are shown in Figures 1c and 1f. Although ocB images are related to the spB images, several key distinctions must be made in our analysis of this reduced result. By limiting the proxy densities to binary values, the radial density fall off that is present in the corona is lost. This discrepancy is accounted for by only analyzing the images at a set radial height. Similarly, the point by point quantitative values obtained via the pB integrations are meaningless without normalization because the applied binary density values have no physical significance. However once normalized, ocB images at set radial heights are comparable to that of pB and spB images.

[12] Bearing these factors in mind, a series of the images is used to construct Carrington maps for spB, ocB, and LASCO C2 pB images. The MAS model is steady state and the resolution is designed to capture the large scale structure of the corona over an entire Carrington rotation. Thus Carrington maps offer a reasonable and appropriate format in which to compare the global corona of the model to the physical corona.

[13] A quantitative method is necessary to objectively compare the three types of Carrington maps that are produced. In this paper a point by point χ^2 calculation is used to assess the correlation of the simulated Carrington maps to observations. Before the χ^2 calculation is applied, two separate normalization schemes are used. In the first scheme, the mean intensity of the poles is subtracted from the data set, and any resulting intensities less than zero are set to zero. This has the effect of removing any DC offset in

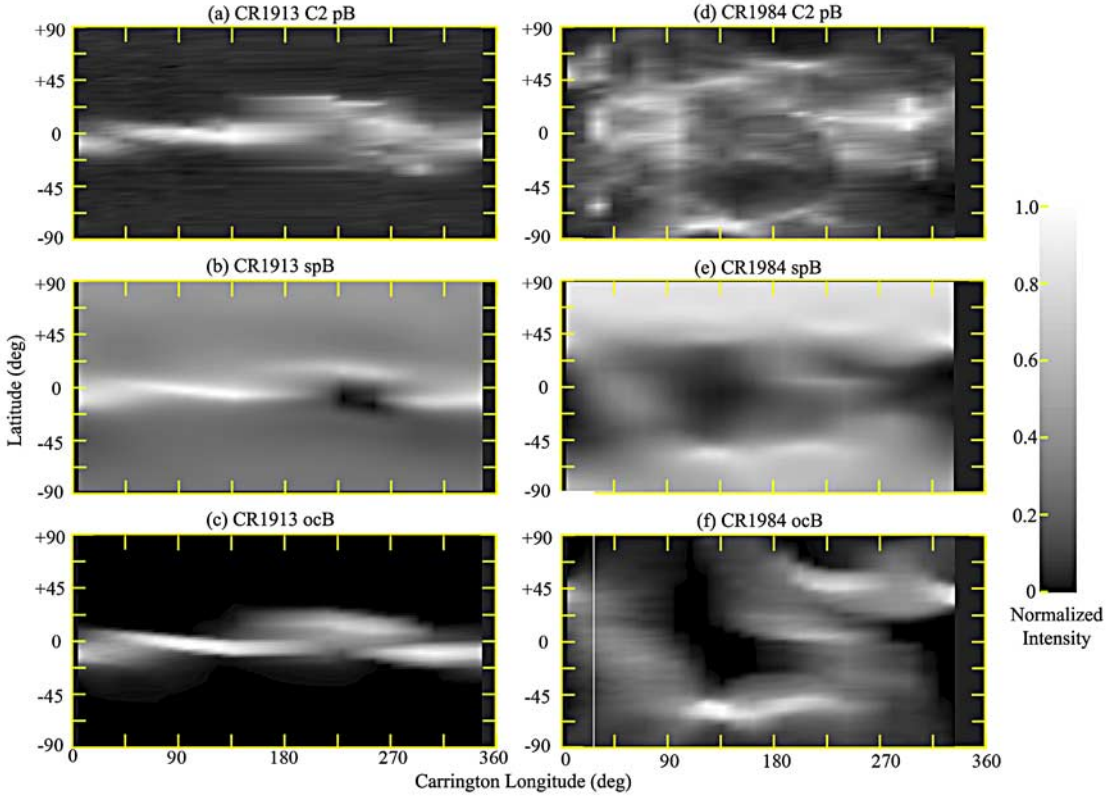

Figure 1. Max/min normalized Carrington maps for CR1913 and CR1984. CR1913 west limb at (a) 3.0 $R_\odot$ LASCO pB, (b) simulated pB, and (c) open-closed brightness. CR1913 occurred between 28 August 1996 and 25 September 1996. CR1984 East Limb at (d) 3.0 $R_\odot$ LASCO pB, (e) spB, and (f) ocB. CR1984 occurred between 3 and 31 December 2001.

the data. The second scheme, normalizes to the intensity range such that,

$$i_{x,y} = \frac{i_{x,y} - i_{\min}}{i_{\max} - i_{\min}} \tag{2}$$

where $i_{x,y}$ is the intensity at pixel (x,y), $i_{\min}$ is the minimum intensity in the map, and $i_{\max}$ is the maximum intensity in the map. Whereas the first scheme results in a translation and rebinning of the intensity distribution, this normalization represents a translation and scaling. The scaling is necessary for comparing ocB to pB because in the process of creating the ocB field we introduced nonphysical units which changed the range of ocB as compared to pB.

[14] The normalized maps are then compared using the χ^2 calculation,

$$\chi^2 = \frac{1}{N} \sum_{x,y} \frac{\left(\mathbb{I}_{x,y} - \mathcal{I}_{x,y}\right)^2}{s^2} \tag{3}$$

$\mathbb{I}$ is the pB intensity, $\mathcal{I}$ is the model's predicted intensity (either spB, ocB, or baseline), s^2 is the variance of the pB map, and N is the number of points in the map. The χ^2 is representative of how closely the density structures of two maps are correlated. The lower the χ^2, the closer the fit between model and data. By applying this calculation to maps at different heights and rotations, we are able to gain a better sense of the model's capabilities at capturing the three-dimensional density structures of the corona.

3. Results

[15] For this study, two Carrington rotations have been examined, CR1913 which occurred between August and September 1996, and CR1984 which occurred between December 2001 and January 2002. These rotations represent the minimum and maximum of solar activity, respectively, as defined by sunspot number. We have chosen to look at these two particular rotations for the drastically different states of the Sun each represents.

[16] Figures 1a–1c show the Carrington maps for CR1913 and Figures 1d–1f show the maps for CR1984. These maps have all been normalized for the reasons discussed in section 2.3. The LASCO pB map for CR1913 shows the typical solar minimum coronal configuration. The long central, bright structure is the streamer belt which is an equatorial region of high density that coincides with the closed field region of the dominant dipole component of the magnetic field. Between 170° and 290° longitude, the streamer belt widens and the intensity at the equator is reduced. This region of the rotation coincides with a large equatorially extended coronal hole that was extensively observed during the Whole Sun Month campaign [*Del Zanna and Bromage*, 1999]. The coronal hole and the nearby equatorial active region, located

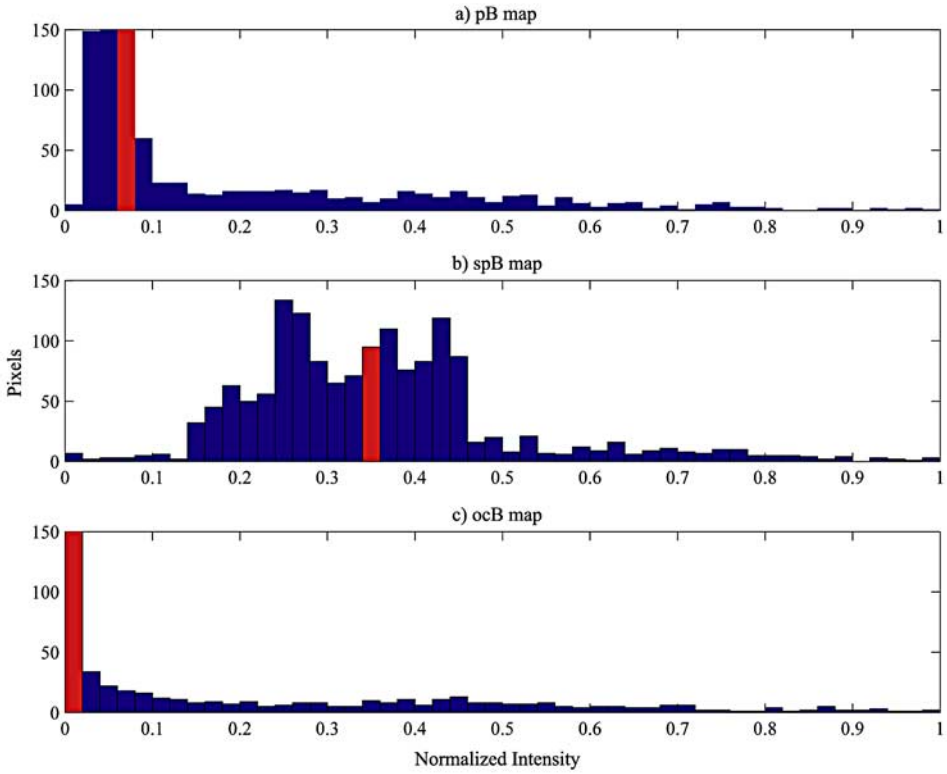

Figure 2. Max/min normalized intensity distribution for CR1913 west limb at 3 $R_{\odot}$: (a) LASCO pB, (b) spB, and (c) ocB. Identical limits are applied to each histogram, although several columns surpass the upper *y* limit. In Figure 2a, the bars centered on 0.05 and 0.07 extend to 586 and 348 pixels, respectively. In Figure 2c, the bar centered on 0.01 extends to 1182 pixels. The red bars mark the mean intensity of the polar regions (±60) in each map.

at 160°, altered the shape of the magnetic neutral line, pushing it northward.

[17] In the spB map for CR1913, the streamer belt is also wider in this region. In comparing the pB and the spB map several key distinctions are apparent. Overall, the spB shows a narrow, almost uniform equatorial streamer belt with longitudinal variations similar to those in the observations. However, the contrast between the polar regions and the streamer belt is much greater in pB than in spB. The poles in the spB maps are still bright. Another striking difference between spB and pB is the location of the intensity minimum. For pB, the minimum is set at the poles, and for spB the minimum is set at the equator near 225° longitude. This equatorial minimum is associated with an active region in the model.

[18] In the CR1913 ocB map, the density contrast in the poles is increased as compared to the spB map. The poles are dark. The dim equatorial spot present in the spB map is replaced by a diffuse medium intensity region. Because the ocB map shows the integral of binary open/closed data along the LOS, it is able to capture the effect of a streamer and coronal hole lying along the same LOS in a realistic, diffuse manner. Qualitatively, there are strong structural similarities between the ocB map and spB map. This is what we expect as both maps are constructed from different variables of the same MHD solution. However, these two maps do differ strongly in the distribution of intensities.

[19] Figure 2 shows the normalized intensity distributions of the same maps displayed in Figures 1a–1c. The pB and ocB maps share a similar distribution shape, which peaks low in the normalized intensity range. However, the ocB distribution peaks at the very minimum of intensity. This is most likely the result of setting the binary value corresponding to open field to null. The spB distribution peaks closer to the middle of intensity range, and its peak is broad. The spB distribution has very few pixels in the low intensity region where pB and ocB distributions peak. The red bars in these histograms mark the mean intensity of the polar regions of the maps. The spB poles are in the midrange of intensity whereas the poles for the pB and ocB maps are near the lower end of the intensity range. These distributions show that the spB intensities are too bright in general, although this is particularly true at the poles. Based on this initial qualitative analysis of the Carrington maps and distributions, the ocB map appears to be a closer fit to the observations in polar and equatorial holes and in overall intensity distribution.

[20] The corona has a much more complicated structure during solar maximum as is seen in comparing the LASCO pB maps for CR1984 and CR1913. The streamers appear discontinuous and scattered. There is a larger area of medium intensities, and overall, structures are more diffuse than in CR1913. The poles are not uniformly dim although smaller coronal holes are still visible in the maps. During maximum activity, the solar magnetic field is more complex.

Table 1. χ^2 for CR1913 and CR1984 at Various Radial Height (χ^2 Formula Is Given in Equation (3))

	Baseline[a]		spB[a]		Baseline[b]		spB[b]		ocB[b]	
Rotation and Height	East	West	East	West	East	West	East	West	East	West
CR1913 2.5 $R_\odot$	1.07	0.738	0.219	0.390	1.06	0.939	2.51	1.95	0.525	0.318
CR1913 3.0 $R_\odot$	0.977	0.724	0.291	0.392	1.37	1.13	3.43	2.38	0.681	0.413
CR1913 4.5 $R_\odot$	0.926	0.677	0.780	0.729	2.34	1.88	3.95	2.98	1.17	0.686
CR1984 2.5 $R_\odot$	0.890	.805	1.17	0.936	2.30	4.23	3.56	9.52	1.78	3.14
CR1984 3.0 $R_\odot$	1.01	0.943	1.27	1.10	2.60	3.67	5.10	9.57	1.91	2.40
CR1984 4.5 $R_\odot$	1.16	1.40	1.27	1.51	3.91	4.95	8.47	12.7	2.12	2.26

[a]Normalized to the intensity of the poles so that $i_{x,y} = \max[0, i_{x,y} - \bar{i}_{pole}]$.
[b]Normalized to the intensity range so that $i_{\min} = 0$ and $i_{\max} = 1$.

In addition to the dipole component, higher multipole moments associated with active regions gain strength. These traits strongly warp the magnetic neutral line, and the streamer belt is most likely transformed into multiple discontinuous streamers at many latitudes.

[21] The spB map for CR1984 contains many individual streamers, although they are less contrasted than in the observations. The poles are bright as they were in the spB map of CR1913. In the ocB map for CR1984, the streamers are more distinct, and the coronal holes are larger in both longitudinal and latitudinal extent than in the spB map. Polar holes are also present. In the spB map, no dark regions occur at latitudes poleward of 60° implying the absence of coronal holes. The ocB map, however, contains a small northern polar hole at 200° to 225° longitude as well as the southern polar hole near 135° longitude. The ocB map suggests that polar coronal holes remain at solar maximum, though they are considerably smaller in area than at solar minimum.

[22] The agreement between the model and the data is not as strong in CR1984 as it was in CR1913. This is to be expected as the corona evolves on shorter timescales and is more active during solar maximum. This affects the accuracy of the synoptic magnetogram used to specify the inner boundary of the model. During solar minimum observational cadence does not introduce as much error as it does during maximum. Transient phenomena such as coronal mass ejections are more common during maximum. These can affect the pB brightness of individual images as well as the overall structure of the corona.

[23] We produced twelve sets of maps similar to those in Figure 1 for both east and west limb of both rotations at 2.5, 3.0, and 4.5 $R_\odot$. We applied the χ^2 calculation and compared the spB and ocB maps to the LASCO pB maps. The two different normalizations described in section 2.3 have been applied. The results are summarized in Table 1 along with the χ^2 for a baseline model based on the work of *Guhathakurta et al.* [1996]. This baseline model was created by fitting pB streamer profiles from the minimum of Solar Cycle 20. Gudhathakurta finds that streamers can be fit using a 3 parameter, height-specific gaussian with a uniform background. We use the best fit parameters at heights of 2.5, 3.0, and 4.5 $R_\odot$ to construct Carrington maps for a time-independent, equatorial streamer. Ideally, a potential field source surface model would serve as a baseline model. However, two characteristics of PFSS models make them undesirable. PFSS models do not output a density, and above the source surface, which is typically placed at 2.35 $R_\odot$ [*Hoeksema et al.*, 1983], all field lines are open. In these ways, PFSS models do not help provide a spB or ocB comparison within the LASCO C2 field of view.

[24] Using the normalization based on the poles, spB has a χ^2 consistently lower than baseline for CR1913 and a comparable χ^2 for CR1984. Using the normalization based on the maximum and minimum intensities, the baseline has a lower χ^2 than spB for all rotations. This descrepancy is a result of the very different effect the two normalization schemes have on the intensity distribution. By normalizing to the poles, the populated bins in the intensity distribution below 0.35 in Figure 2b are summed and deposited in the bin representing the mean polar intensity. This creates a distribution which more closely resembles Figure 2a. The polar normalization sidesteps the problem the MAS model has with dim equatorial regions. The result is a lower χ^2.

[25] The maximum/minimum normalization is necessary to compare ocB to the data. By using binary proxy densities, we have changed the range of the intensity distribution of ocB as compared to pB. The maximum/minimum normalization translates and scales the ocB distribution so that it is comparable to the pB. If the shape of the spB distribution were similar to that of pB, this normalization should result in a spB χ^2 lower than baseline. However, Figure 2 shows that the distribution of spB is much flatter than pB. Using the maximum/minimum normalization, the ocB maps exhibit a lower χ^2 than the spB maps for every rotation. The range of improvement varies from a factor of 2–4. The comparison between ocB and the baseline model is less dramatic. The ocB maps have a χ^2 lower than baseline by a factor of 1.3–2.0, and the improvement for ocB over baseline is reduced in CR1984. Overall, both MAS and the baseline better capture coronal structure in CR1913 than CR1984. The spB fit is particularly off in CR1984, with χ^2 double that of the baseline in some instances. We do not expect that the baseline model should fit particularly well for CR1984 because it is a axisymmetric model which is not realistic for the magnetic structure of solar maximum. In regards to variations between the limbs, there does not seem to be a pattern over all maps and both normalizations. It is typical for one limb to have consistently lower χ^2 for all heights in a given rotation and model. This may be attributed to transient phenomena captured in the C2 data. Logically, there should not be a preferred limb in terms of fitting accuracy.

[26] In general, the χ^2 increases with radial height. This effect is caused by the geometric narrowing of streamers with height. Because the outer corona is mostly open at

4.5 $R_\odot$, there are many more points near the minimum intensity than the maximum, and the only density enhancements are directly surrounding the current sheet. Any small positional errors in the location of the neutral line therefore have large effects on the χ^2.

[27] Table 1 clearly illustrates that the MAS model is capable of recreating the structure of the corona. Although, the density and the unnormalized simulated polarization brightness do not accurately reproduce the LASCO maps, the magnetic structure of the model is consistent with the observed data. When logically normalized, spB is an improvement over the baseline.

4. Discussion

[28] Currently, computational limitations still affect the order of the approximations that must be applied to make the problem of modeling the solar corona tractable. As computers and models continue to grow in complexity, there is a necessity to assess and track our progress at understanding the physics that dominate the corona. The metric developed in this paper can serve as gauge for that purpose.

[29] The terms in the energy equation used in MHD simulations can have drastic effects on the solution. To zeroth order, the corona is assumed to be isothermal. To first order, a polytropic assumption is reasonable. However, with these approximations anisotropic conduction, radiative cooling, and explicit coronal heating are all neglected. Density is particularly sensitive to these higher order terms. Any model not including them will not likely be able to accurately simulate white light scattering images based on model densities. However, because the corona is magnetically dominated, these higher order effects are less likely to have a strong effect on the magnetic field configuration. In exclusively using the model's magnetic field solution, subject to a LOS integral, to produce ocB images, this metric is able to look past the known shortcomings of this particular type of model and assess how well it captures the magnetic structure of the corona. Versions of the MAS model are being developed which implement a more detailed energy equation [*Linker et al.*, 2007]. When this metric is applied to more realistic models, we expect the χ^2 for the spB maps should decrease as compared to those found in this paper. The ocB χ^2 should not change drastically, however, because the magnetic field is dominant over thermodynamics in the low β-corona.

[30] The most obvious shortcoming of the spB is the latitudinal intensity profile. The intensity in the polar regions is too high, and the intensity minimum is found near equatorial holes. This effect can be attributed to dynamical effects of flux tube geometries. In the model some small equatorial coronal holes are rooted in active regions. Even if a small percentage of the flux of these active regions is open, the strong magnetic field of these regions forces a dramatic expansion of these flux tubes in the lower corona. In a model based on a polytropic gas, this rapid expansion greatly decreases the density of the flux tube. Because the boundary conditions of the model are uniform at the coronal base, this rapid near-surface expansion greatly reduces the density near equatorial active regions as compared to the slowly expanding polar flux tubes. It is likely that the inclusion of more sophisticated thermodynamics will provide more accurate density profiles.

5. Conclusions

[31] A quantitative metric is necessary to assess the growth and abilities of MHD models of the solar corona. We have created a metric that is capable of analyzing the MHD solutions through two distinct and complementary methods. Simulated polarization brightness (spB) images and open-closed brightness (ocB) images can both be compared to observational polarization brightness data through the creation of normalized Carrington maps. Using a χ^2 comparison we find that the ocB maps matched the data more closely than the spB maps. This is expected with the limited thermodynamics of the MAS model. The model more accurately captured the white light structures during CR1913 than during CR1984. Even during CR1984, the ocB map shows that the model captures the overall structure of the corona well as indicated by the significantly lower χ^2 than that of a baseline model. The next generation of global coronal MHD is currently in its early stages, but we plan on carrying out further analysis on these upcoming model results. An augmented energy equation should greatly enhance the accuracy of the model's density prediction. There is also community interest in incorporating vector magnetogram boundary conditions in global MHD. This might have drastic effects on magnetic structure and ocB predictions. Another application of this analysis is in the inner corona using the HAO Mark IV coronagraph. In this approach, a comparison with a PFSS model can be made similar to that of *Riley et al.* [2006a, 2006b]. This metric is widely applicable to coronal MHD models and is a viable tool for the space physics community as it attempts to create predictive space weather models.

[32] **Acknowledgments.** We thank Joan Burkepile and Janet Luhmann for useful discussions. This work was supported by the Center for Integrated Space weather Modeling, which is funded by the STC program of the National Science Foundation under Agreement number ATM-0120950. SOHO is a joint project of the European Space Agency and NASA. HAO/NCAR is sponsored by the National Science Foundation. An earlier version of this formed the senior distinction thesis of DJS at Boston University.

[33] Amitava Bhattacharjee thanks Adam Szabo and another reviewer for their assistance in evaluating this paper.

References

Billings, D. E. (1966), *Guide to the Solar Corona*, Academic Press, New York.

Del Zanna, G., and B. J. I. Bromage (1999), The Elephant's Trunk: Spectroscopic diagnostics applied to SOHO/CDS observations of the August 1996 equatorial coronal hole, *J. Geophys. Res.*, *104*(A5), 9753–9766.

Guhathakurta, M., T. Holzer, and R. M. MacQueen (1996), The Large-Scale Density Structure of the Solar Corona and the Heliospheric Current Sheet, *Astrophys. J.*, *458*, 817–831.

Hoeksema, J. T., J. M. Wilcox, and P. Scherrer (1983), The structure of the heliospheric current sheet: 1978–1982, *J. Geophys. Res.*, *88*(A12), 9910–9918.

Hundhausen, A. J. (1993), Sizes and locations of coronal mass ejections, *J. Geophys. Res.*, *98*(A8), 13,177–13,200.

Lee, C. O., J. Luhmann, D. Odstrcil, P. MacNeice, I. de Pater, P. Riley, and C. N. Arge (2009), The solar wind at 1 AU during the declining phase of solar cycle 23: Comparison of 3D numerical model results with observations, *Sol. Phys.*, *254*, 155–183.

Linker, J. A., Z. Mikić, D. A. Biesecker, R. J. Forsyth, S. E. Gibson, A. J. Lazarus, A. Lecinski, P. Riley, A. Szabo, and B. J. Thompson (1999), Magnetohydrodyanmic modeling of the solar corona during Whole Sun Month, *J. Geophys. Res.*, *104*(A5), 9808–9830.

Linker, J. A., R. Lionello, Z. Mikic, P. Riley, and V. Titov (2007), Thermodynamic MHD Modeling of Coronal Mass Ejections, paper presented at American Astronomical Society Meeting 210, Honolulu, Hawaii.

McGregor, S. L., W. J. Hughes, C. N. Arge, and M. Owens (2008), Analysis of the magnetic field discontinuity at the potential field source surface and Schatten Current Sheet interface in the Wang-Sheeley-Arge model, *J. Geophys. Res.*, *113*(A8), A08112, doi:10.1029/2007JA012330.

Owens, M., C. N. Arge, H. Spence, and A. Pembroke (2005), An event-based approach to validating solar wind speed predictions: High-speed enhancements in the Wang-Sheeley-Arge model, *J. Geophys. Res.*, *110*, A12105, doi:10.1029/2005JA011343.

Riley, P., J. A. Linker, and Z. Mikic (2002), Modeling the heliospheric current sheet, *J. Geophys. Res.*, *107*(A7), 1136, doi:10.1029/2001JA000299.

Riley, P., J. A. Linker, Z. Mikic, R. Lionello, S. Ledvina, and J. Luhmann (2006a), A comparison between global solar MHD and potential field source surface model results, *Astrophys. J.*, *653*, 1510–1516.

Riley, P., J. A. Linker, Z. Mikic, and D. Odstrcil (2006b), Modeling interplanetary coronal mass ejections, *Adv. Space Res.*, *38*, 535–546, doi:10.1016/j.asr.2005.04.040.

Saito, K., A. I. Poland, and R. H. Munro (1977), A study of the background corona near solar minimum, *Sol. Phys.*, *55*, 121–134.

Spence, H., D. Baker, A. Burns, T. Guild, C. L. Huang, G. Siscoe, and R. Weigel (2004), Center for integrated space weather modeling metrics plan and initial model validation results, *J. Atmos. Sol.-Terr. Phys.*, *66*, 1499–1507.

G. de Toma, S. Gibson, and M. Wiltberger, High Altitude Observatory, National Center for Atmospheric Research, P.O. Box 3000, Boulder, CO 80305, USA.

W. J. Hughes and H. Spence, Center for Space Physics, Boston University, 725 Commonwealth Avenue, Boston, MA 02215, USA.

J. A. Linker, Z. Mikic, and P. Riley, Solar Physics Group, Predictive Science Incorporated, 9990 Mesa Rim Road, Suite 170, San Diego, CA 92121, USA.

D. J. Schmit, Department of Astrophysical and Planetary Science, University of Colorado, UCB 391, Boulder, CO 80309, USA. (donald.schmit@colorado.edu)